Title
Elucidating Driving Forces for Liposome Rupture: External Perturbations and Chemical Affinity

Journal
Langmuir, 28(19)

ISSN
0743-7463

Authors
Wang, Xi
Shindel, Matthew M
Wang, Szu-Wen
et al.

Publication Date
2012-05-15

DOI
10.1021/la300127m

Langmuir

Article

pubs.acs.org/Langmuir

Elucidating Driving Forces for Liposome Rupture: External Perturbations and Chemical Affinity

Xi Wang, Matthew M. Shindel, Szu-Wen Wang, and Regina Ragan*

Department of Chemical Engineering and Materials Science, University of California, Irvine, California 92697-2575, United States

Supporting Information

ABSTRACT: Atomic force microscopy (AFM) studies under aqueous buffer probed the role of chemical affinity between liposomes, consisting of large unilamellar vesicles, and substrate surfaces in driving vesicle rupture and tethered lipid bilayer membrane (tLBM) formation on Au surfaces. 1,2-Distearoyl-*sn*-glycero-3-phosphoethanolamine-*N*-poly-(ethylene glycol)-2000-*N*-[3-(2-pyridyldithio) propionate] (DSPE-PEG-PDP) was added to 1-palmitoyl-2-oleoyl-*sn*-glycero-3-phosphocholine (POPC) vesicles to promote interactions via Au−thiolate bond formation. Forces induced by an AFM tip leading to vesicle rupture on Au were quantified as a function of DSPE-PEG-PDP composition with and without osmotic pressure. The critical forces needed to initiate rupture of vesicles with 2.5, 5, and 10 mol % DSPE-PEG-PDP are approximately 1.1, 0.8, and 0.5 nN, respectively. The critical force needed for tLBM formation decreases from 1.1 nN (without osmotic pressure) to 0.6 nN (with an osmotic pressure due to 5 mM of $CaCl_2$) for vesicles having 2.5 mol % DSPE-PEG-PDP. Forces as high as 5 nN did not lead to LBM formation from pure POPC vesicles on Au. DSPE-PEG-PDP appears to be important to anchor and deform vesicles on Au surfaces. This study demonstrates how functional lipids can be used to tune vesicle−surface interactions and elucidates the role of vesicle−substrate interactions in vesicle rupture.

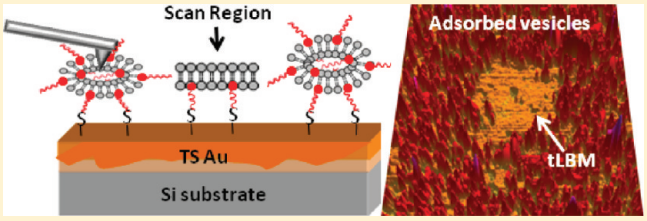

INTRODUCTION

Phospholipid bilayer membranes (LBMs), since their introduction by McConnell's group,[1] have attracted great interest as model cell membranes,[2−4] which can be used to study cell surface properties or cell surface interactions,[5−8] T-cell receptor and antigen presentation,[9,10] and membrane phase behavior.[11] There is a significant body of literature investigating the mechanical stability of solid supported LBMs[1,6] and engineering lipid lateral mobility using polymer cushions[2,3,12,13] and lipopolymer tethers to LBMs[14−19] to mimic cell behavior. When LBMs are assembled on conducting substrates such as Au, they have applications as biosensors for measuring protein−lipid interactions and protein−protein recognition via a change in electrical[20,21] or optical response.[21−24] Potassium or calcium ion transport across membranes containing gramicidin[25] or valinomycin[17,19] ion channels has been probed with impedance spectroscopy using the conductive substrate as a counter electrode. These LBM systems can also be used to measure light-activated proton transport[26] for energy applications.[27,28] Thus, LBM assembly on metal surfaces yields a high degree of functionality.

Although vesicle fusion on insulating, hydrophilic surfaces[29] such as mica[30,31] or glass[32,33] has been widely reported to lead to LBMs, vesicle fusion does not occur on Au surfaces in the absence of chemical functional groups.[34] Vesicle fusion has been performed on chemically functionalized Au using multistep processing methods such as self-assembled monolayer formation[35−38] and Langmuir−Blodgett transfer[39−41] prior to vesicle fusion. Recently, Wang et al. reported a simplified protocol utilizing 1,2-distearoyl-*sn*-glycero-3-phosphoethanolamine-*N*-poly(ethylene glycol)-2000-*N*-[3-(2-pyridyldithio) propionate] (DSPE-PEG-PDP) in 1-palmitoyl-2-oleoyl-*sn*-glycero-3-phosphocholine (POPC) vesicles to promote tethered LBMs (tLBMs) formation on bare template-stripped (TS) Au surfaces[42] where the functional group, PDP, was incorporated in POPC vesicles to form Au−thiolate bonds at the surface.[36,42] In this study, atomic force microscopy (AFM) force spectroscopy that has piconewton force sensitivity[43−45] is performed to examine the role of functional groups incorporated in vesicles to promote increased vesicle−substrate interactions and to understand how this affects the initiation of tLBM formation. Vesicle fusion and the resulting LBM formation generally involve three stages: (i) adsorption of vesicle on substrate surfaces; (ii) fusion of neighboring adsorbed vesicles to form larger vesicles; (iii) vesicle rupture for the formation of LBM domains, where stage (ii) and (iii) may take place independently, consecutively, or simultaneously.[30,34,46−48] LBM formation via vesicle fusion has been heavily examined in terms of a critical vesicle concentration or a critical size needed for fusion and rupture. Yet it has also been observed that the critical concentration and size varies for different material systems,[34,47,49−53] and thus the vesicle−substrate interaction clearly plays a role. There have been some theoretical studies indicating the importance of vesicle−

Received: January 9, 2012
Revised: April 13, 2012
Published: April 17, 2012

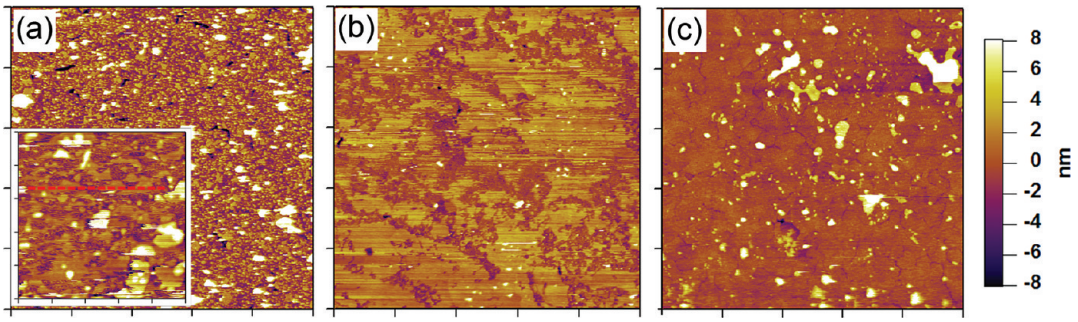

Figure 1. 5 μm × 5 μm AFM topography images of TS Au after exposure to (a) 2.5% DSPE-PEG-PDP/97.5% POPC vesicles for 30 min incubation at room temperature, (b) 10% DSPE-PEG-PDP/90% POPC vesicles for 30 min incubation at room temperature, and (c) 2.5% DSPE-PEG-PDP/97.5% POPC vesicles for 30 min incubation at room temperature followed by 30 min incubation at 60 °C. The inset in panel a is a 1 μm × 1 μm AFM topography image obtained after a 30 min incubation period at room temperature with 2.5% DSPE-PEG-PDP/97.5% POPC vesicles. The line profile corresponding to the red dashed line in the inset is shown in Supporting Information Figure S1b.

substrate interactions,[54] yet systematic experimental studies varying this parameter are rare.[55]

Since the mechanical force applied via an AFM tip was found to affect tLBM formation dynamics on TS Au, tip-induced forces can be used for selective LBM formation and for examining critical forces for initiating rupture of vesicles. In our investigation, the required external force associated with promoting tLBM formation in aqueous buffer on Au was quantified using AFM force spectroscopy for vesicles without functional lipids and with three different concentrations of functional lipids. The functional lipids play a critical role in anchoring vesicles to the surface. Via AFM imaging and force spectroscopy measurements, we also find that increasing the number of functional groups in vesicles, and thereby increasing the chemical affinity between vesicles and substrate surfaces, lowers the required force to initiate tLBM formation. Increased vesicle−substrate interactions are expected to lead to deformation of vesicles and lower the activation energy for rupture as predicted by fracture theory.[49] While in the absence of functional lipids, osmotic pressure does not lead to tLBM;[51] here osmotic pressure was found to lower the critical force leading to rupture of vesicles with functional lipids. In addition to further understanding vesicle rupture mechanics on Au surfaces, this investigation provides a means for comparing vesicle rupture mechanics in a multitude of systems. For example, exosomes and liposomes are potential vehicles for gene delivery and drug delivery,[56−58] and understanding mechanisms for triggered release of the internal payload from the vesicular structures under specific conditions such as ultrasound[59,60] and thermo sensitivity[61] is critical. This study of vesicle rupture mechanics also provides a means for elucidating the nanomechanical properties of vesicles that are crucial for biological activities such as cell membrane fusion and endocytosis.[56,62,63]

MATERIALS AND METHODS

Materials. POPC and DSPE-PEG-PDP were obtained from Avanti Polar Lipids (Alabaster, AL). HEPES at >99.5% purity and chloroform at >99.8% purity were purchased from Sigma-Aldrich (St. Louis, MO). NaCl at >99.0% purity and $CaCl_2$ at >95.0% purity were from Fisher Scientific Inc. (Pittsburgh, PA). Au pellets with 99.99% purity were obtained from Kurt J. Lesker Company (Clairton, PA). Silicon wafers were purchased from University Wafer (South Boston, MA). Two-component epoxy glue, EPO-TEK 377H, was purchased from Epoxy Technology, Inc. (Billerica, MA). Au pellets were used to deposit continuous metal films on silicon wafers, and the epoxy was used for bonding TS Au to Si substrates. All water used in this study was purified with a Milli-Q water system (≥18.2 MΩ.cm, Millipore Corp., Billerica, MA). All chemicals were used as received.

Preparation of Unilamellar Vesicles. Large unilamellar vesicles were prepared following an extrusion method.[39,64] Vesicles with lipid composition of (i) 0 mol % DSPE-PEG-PDP/100 mol % POPC, (ii) 2.5 mol % DSPE-PEG-PDP/97.5 mol % POPC, (iii) 5 mol % DSPE-PEG-PDP/95 mol % POPC, and (iv) 10 mol % DSPE-PEG-PDP/90 mol % POPC were prepared. DSPE-PEG-PDP and POPC lipids were dissolved in chloroform at 1 mg/mL for stock solutions. Lipids were mixed at specified molar ratios for further use. The lipids in chloroform mixture were dried on the bottom of a glass vial by a gentle stream of nitrogen and desiccated in vacuum for at least 1 h. Then, the dried lipid mixtures were rehydrated by the addition of HEPES buffer (5 mM HEPES, pH 7.4, with 150 mM NaCl) to yield a final lipid concentration of 5 mM. The resulting lipid suspensions were then rigorously vortexed, subjected to five freeze−thaw cycles, and extruded 15 times through two polycarbonate membranes with a pore size of 100 nm using a syringe-type extruder (Avanti Polar Lipids, Alabster, AL). The size of vesicles was characterized by dynamic light scattering (Malvern Zetasizer ZS) to have an average diameter of 120 nm with a polydispersity index of less than 0.2.

Preparation of TS Au Substrate. TS Au substrates were prepared following a simplified protocol established by Lee et al.[65] Continuous Au films of 500 nm thick were deposited by electron beam deposition (rate 0.1−2 Å/s, 2.5 × 10^{-6} Torr) on silicon templates with a thermally oxidized SiO_2 layer of approximately 10 nm thick. Prior to transfer, Au films on silicon template were annealed at 200 °C for 24 h under ambient conditions to facilitate grain growth and decrease surface roughness.[66] Then, annealed Au films were glued to a silicon substrate with EPO-TEK 377H epoxy and cured at 150 °C for 1 h to form a sandwich structure. After cooling, silicon templates were stripped off from silicon substrates to expose a pristine TS Au surface with a root-mean-square roughness of less than 0.6 nm over a 2 μm × 2 μm area as evaluated by AFM. TS Au surfaces were used immediately after stripping to maintain a pristine surface for LBM assembly.

Preparation of tLBMs. A 100 μL aliquot of vesicle suspension in HEPES buffer with lipids composition of (i) 0% DSPE-PEG-PDP/100% POPC, (ii) 2.5% DSPE-PEG-PDP/97.5% POPC, (iii) 5% DSPE-PEG-PDP/95% POPC, or (iv) 10% DSPE-PEG-PDP/90% POPC was deposited on an 8 mm × 8 mm TS Au substrate glued on a glass slide. All samples were incubated at room temperature for 30 min. After room-temperature incubation, some samples were immersed in 6 mL HEPES buffer preheated to 60 °C and incubated at 60 °C for another 30 min in an EchoTherm programmable digital chilling incubator (Torrey Pines Scientific, Inc., San Marcos, CA). All samples were rinsed with 200 μL of HEPES buffer four times and glued to a glass slide for AFM characterization after incubation. Sample surfaces were kept hydrated in HEPES buffer during AFM characterization.

dx.doi.org/10.1021/la300127m | *Langmuir* 2012, 28, 7417−7427

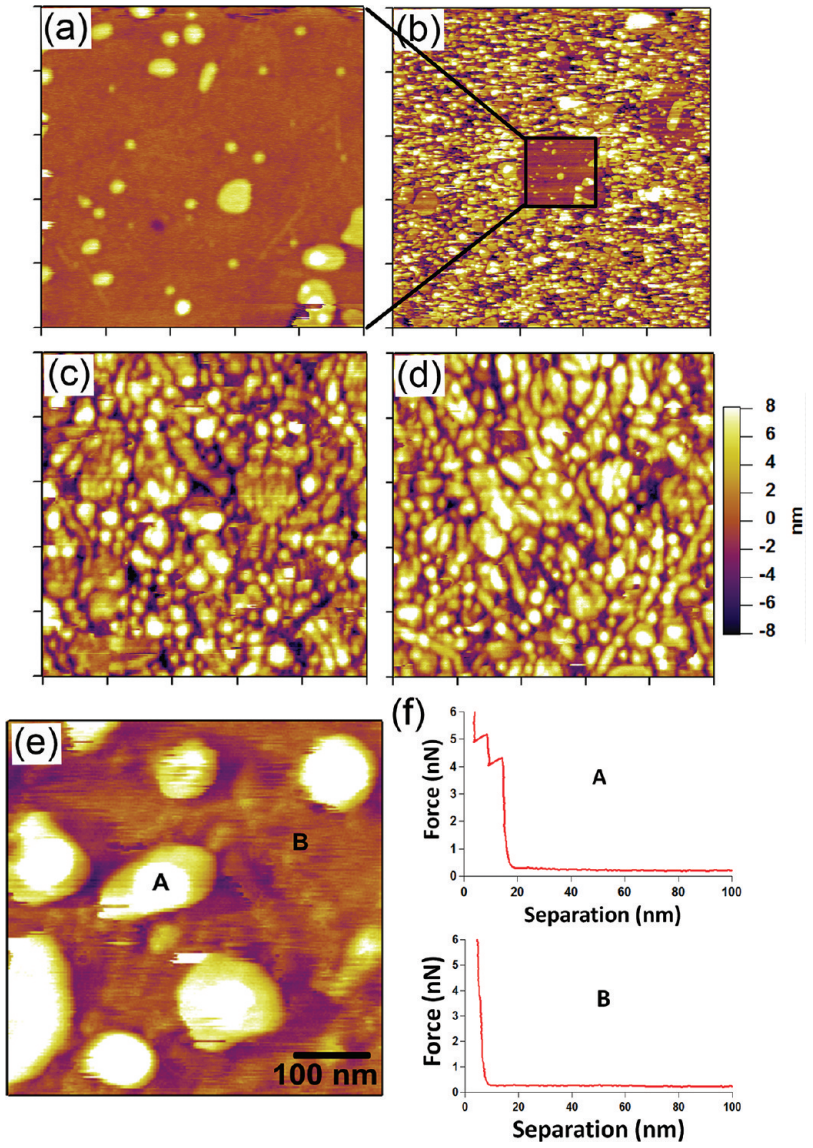

Figure 2. (a) 1 μm × 1 μm AFM topography images of TS Au after exposure to 2.5% DSPE-PEG-PDP/97.5% POPC vesicles for 30 min at room temperature and after 20 min of continuous AFM scanning. (b) 5 μm × 5 μm AFM topography image where the scan region of panel a is highlighted with a black square. (c,d) 1 μm × 1 μm AFM topography images of 100% POPC on oxygen plasma treated TS Au after a 30 min incubation period at room temperature and after 20 min of continuous tapping mode scanning, respectively. (e) Higher resolution AFM topography image of POPC/TS Au obtained after 20 min of continuous tapping-mode scanning. (f) Force–distance curves corresponding to two areas shown in panel (e).

AFM Imaging and Force Spectroscopy. Both AFM imaging and force spectroscopy were performed using a MFP-3D-Bio AFM (Asylum Research, Santa Barbara, CA). Commercial AFM tips with a pyramid-shaped Si_3N_4 cantilever, Au coating on the reflective side of the tips (OMCL-TR 400 PSA, Olympus), and a nominal spring constant of 0.08 N/m were used for all AFM measurements. Both AFM imaging and force spectroscopy were carried out at room temperature in HEPES buffer. AFM images were acquired under tapping mode with a scan speed of 1.0 Hz. All topography images contain 512 × 512 pixels and were rendered with background slopes corrected using *Igor Pro* software v 6.0.

AFM force spectroscopy was performed under contact mode. Before each force map, AFM cantilever spring constants were calibrated by measuring deflection against a hard reference substrate and then by the thermal noise method.[67] Force spectroscopy maps were performed in a 1 μm × 1 μm region. At each pixel location, an individual force–distance curve composed of an extension-retraction cycle was acquired. In each force–distance measurement cycle, AFM tip retraction was initiated at a specified maximum force, referred to as the trigger force. This allows for control of the applied force by the AFM tip. The breakthrough distance, the discontinuity in the force–distance curve as the tip penetrates the membrane or vesicle surface, was measured from the data in the extension part of the force–distance curves. Histograms of breakthrough distance data extracted from force maps on similar sample surfaces with a trigger force of 5 nN were generated.

RESULTS AND DISCUSSION

tLBM Formation on TS Au. Figure 1a shows a 5 μm × 5 μm AFM topography image of a TS Au surface after room-temperature incubation with 2.5% DSPE-PEG-PDP/97.5% POPC vesicle suspension. AFM imaging was performed immediately after incubation. The inset is a 1 μm × 1 μm AFM topography image that highlights the surface features. A reference AFM topography image of bare TS Au is shown in Supporting Information Figure S1a. A line profile along the region highlighted with a dashed line in Figure 1a, shown in Supporting Information Figure S1b, has features with a relative

dx.doi.org/10.1021/la300127m | *Langmuir* 2012, 28, 7417–7427

height of 5.1 nm, indicating partial coverage of tLBM in this region.[42,68] Adsorbed vesicles have larger feature heights, in the range of the thickness of a double bilayer. Thus in Figure 1a, a mixture of features is observed on the surface: bare Au regions, adsorbed vesicles, and tLBM patches. Spontaneous tLBM formation with vesicles in the absence of chemical functional groups is not observed on Au surfaces, and vesicles do not adsorb or remain intact on native and oxidized Au surfaces.[34,51] Wang et al. have shown previously that tLBMs will form on native Au upon exposure to vesicles with functional lipids, DSPE-PEG-PDP, and will not form when exposed to pure POPC vesicles.[42] However, here we see that at short incubation times the formation is incomplete for vesicles containing DSPE-PEG-PDP, and this can be observed during the first AFM scan immediately after incubation. Longer incubation times generally result in more continuous coverage. Furthermore, AFM scanning can lead to further tLBM formation, *vide infra*, that is observed in subsequent scans. By increasing the concentration of DSPE-PEG-PDP in POPC vesicles to 10%, we find a larger coverage of tLBM on the surface when prepared and imaged under similar conditions as in the 5 μm × 5 μm AFM topography image of Figure 1b.

In order to promote continuous tLBM coverage, a TS Au substrate was incubated with 2.5% DSPE-PEG-PDP/97.5% POPC vesicle suspension at room temperature and then incubated at 60 °C[51,69] while being hydrated in HEPES buffer. A 5 μm × 5 μm AFM topography image of this sample is shown in Figure 1c. The AFM image in Figure 1c has flat regions coexisting with higher topographic features that appear white. Other AFM images acquired on the sample surface exhibit similar topography. Force spectroscopy was performed on the flat regions, and consistent breakthrough events with breakthrough distances of 4.2 ± 0.7 nm (1 σ, n = 1000) were observed, indicating the presence of a tLBM on TS Au. A representative force−distance curve is shown in the Supporting Information, Figure S1c. The white features are consistent with flattened adsorbed vesicles on a tLBM background when evaluating the size and shape of the line profile of these features. (See Supporting Information Figure S1d.) Thus, large area formation of continuous tLBM is possible by sample incubation at 60 °C. Increasing temperature to promote LBM formation[25,70] is hypothesized to be associated with increased vesicle−vesicle interactions leading to vesicle fusion or thermally activated vesicle rupture thereby reducing the critical coverage required for tLBM.[51] To clarify, here we differentiate between vesicle fusion and LBM formation. Vesicle fusion is used in the literal sense: the fusion of two or more vesicles. tLBM formation over large areas under elevated temperature, and not at room temperature, indicates that vesicle rupture on Au has slow kinetics[49,50] or is thermodynamically unfavorable at room temperature. The data of Figure 1a,b showing tLBM patches on the surface after room-temperature incubation indicates that in this system vesicle rupture is kinetically hindered and thermally activated.

Mechanically Induced tLBM Formation. The slow vesicle rupture kinetics on TS Au at room temperature allows for study of mechanisms inducing vesicle rupture using AFM. Figure 2a shows 1 μm × 1 μm AFM topography images of TS Au after exposure to vesicles composed of 2.5% DSPE-PEG-PDP/97.5% POPC after 20 min of continuous AFM scanning (two complete scans). In comparison to Figure 1a, where tLBM patches and adsorbed vesicles are observed alongside bare TS Au surfaces, a relatively uniform tLBM is observed in Figure 2a, where the AFM tip has scanned the surface. When the scan size on the same region is increased to 5 μm × 5 μm, as shown in Figure 2b, only the 1 μm × 1 μm region near the center (outlined with a black square) that had been scanned by the AFM tip shows a continuous tLBM in the image and in force−distance measurements. The neighboring regions, outside the scan area, are predominantly covered by adsorbed vesicles coexisting with small tLBM and bare Au regions. This indicates that the external force applied by the AFM tip during imaging induces rupture of adsorbed vesicles[54] and thus facilitates tLBM formation on Au that can be observed in subsequent scans. Analogous measurements were performed on vesicles composed of 100% POPC that were incubated on oxygen plasma-treated TS Au. Au was plasma cleaned in this case since POPC vesicles will not adsorb on untreated Au surfaces.[42,51] AFM topography images were acquired immediately after incubation and after scanning for 20 min (two complete scans). These images are shown in Figure 2c,d, respectively. Comparison of these two images shows that the surface morphology did not change significantly after interactions with the AFM tip during scanning. A higher resolution image is shown in Figure 2e, and representative force−distance curves on the labeled regions are shown in Figure 2f. After AFM scanning, force−distance measurements in region A show double breakthrough events (absorbed vesicles), and in region B they show no breakthrough events (bare Au regions). Thus the lack of LBM from POPC demonstrates it is not the interaction between the vesicles and the AFM tip alone that is responsible for tLBM formation but that the functional lipids, DSPE-PEG-PDP, are needed.

In order to monitor the evolution of features on the surface in response to interactions with the AFM tip, force spectroscopy was performed over a 1 μm × 1 μm region in 32 × 32 arrays with a trigger force of 5 nN. A force of 5 nN is known to penetrate tLBMs, adsorbed vesicles, and multilayers, and the measured breakthrough distance differentiates the features.[42] Three consecutive 1 μm × 1 μm force maps were performed on a sample after incubation with vesicles containing 2.5% DSPE-PEG-PDP/97.5% POPC on TS Au; 1024 individual force−distance curves were collected in the 32 × 32 arrays in the force mapping region. The measured breakthrough distances from the acquired force−distance curves are plotted as a histogram in Figure 3a−c, corresponding to the first, second, and third force map, respectively. Force−distance curves with a measured breakthrough distance of zero represent the interaction of the tip with a hard surface.[71] The blue arrow marks the force−distance curves with a measured breakthrough distance between 4.4 ± 0.5 nm (1 σ, n = 2035), which is consistent with the thickness of a tLBM. The black triangle marks the force−distance curves having a measured breakthrough distance of 9.3 ± 0.8 nm (1 σ, n = 519), indicating the presence of adsorbed vesicles or multilayers.[42,68] The histograms show that from the first, to the second, to the third force map, the percentage of force−distance curves having a mean breakthrough distance of 4.4 nm (tLBM) increases from 25%, 37% to 48%, respectively, and the percentage of force−distance curves having a mean breakthrough distance of 9.3 nm (adsorbed vesicles) decreases from 19%, 7% to 4%, respectively. Clearly, the interaction with the AFM tip during force spectroscopy induces vesicle rupture/tLBM formation.

Breakthrough events with a distance of zero appear to occur due to interaction of the tip with bare Au surface as well as due to disruption of the tLBM caused by force−distance measure-

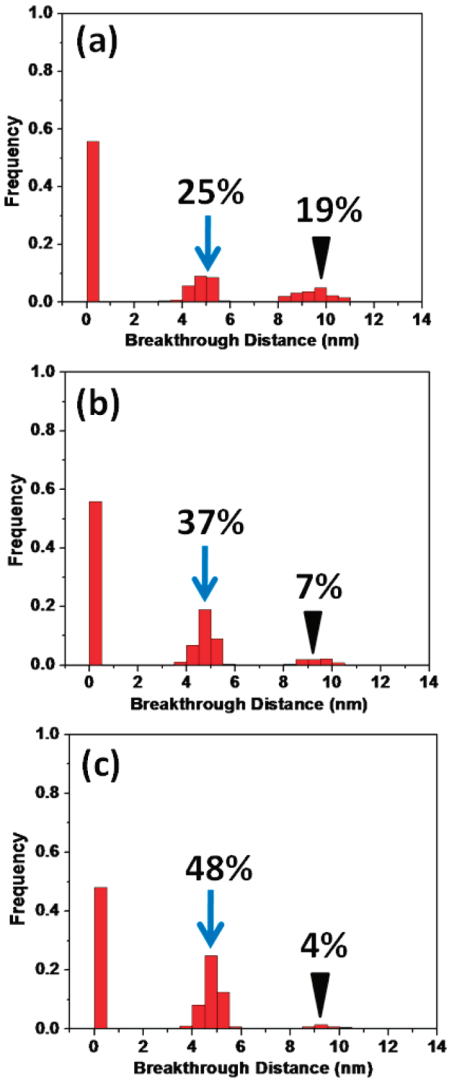

Figure 3. Histograms of measured breakthrough distances from acquired force spectroscopy data using a trigger force of 5 nN on TS Au after 30 min of room-temperature incubation with 2.5% DSPE-PEG-PDP/97.5% POPC vesicles. Data shown in a, b, and c are from three consecutive force maps that were performed in the same 1 μm × 1 μm region on the sample surface. The blue arrows mark the peak with an average breakthrough distance of 4.4 ± 0.5 nm (1 σ, n = 2035); black triangles mark the peak with an average breakthrough distance of 9.3 ± 0.8 nm (1 σ, n = 519).

ments at neighboring locations. Figure S2 in the Supporting Information shows that the number of zero breakthrough events decreases as the spacing between neighboring force–distance measurements increases. While some of the zero breakthrough events are due to disruption of the tLBM caused by force–distance measurements in the 32 × 32 arrays force maps, the monotonic decrease of zero breakthrough events with consecutive force mapping observed in Figure 3 indicates that there are less bare regions on the surface due to tip–surface interactions. It is interesting to note that the pixel size in the force map array is 31.3 nm × 31.3 nm, and the average vesicle diameter as prepared is 100 nm; thus during force mapping, vesicles have multiple interactions with the tip. Although 5 nN is sufficient force to penetrate a vesicle, the continued decrease of breakthrough events corresponding to vesicles on the surface after the first force map shows that, in some cases, multiple interactions between the tip and the surface are needed for vesicle rupture. Thus, the evolution of features on the surface observed in Figure 3 indicates that vesicle rupture due to interaction with the tip is a statistical event, and vesicles may heal after penetration.

Analogous experiments were performed on 100% POPC vesicles on plasma-cleaned TS Au. After the first force map was performed with a trigger force of 5 nN, a bare 1 μm × 1 μm region remained in the force mapped region (see Supporting Information Figure S3a-1). In a different region, the trigger force was lowered to 1 nN, a 1 μm × 1 μm region was force mapped, and again a bare Au surface remained in the force mapped region (see Supporting Information Figure S3b-1). Thus POPC vesicles are no longer evident on the surface after applying force with the AFM tip that has been observed previously when imaging with a high tapping-mode set point.[54] Overall, without DSPE-PEG-PDP functional lipids, comparable external force exerted on vesicles does not induce tLBM formation on TS Au. The fact that POPC vesicles leave the surface when subjected to forces comparable to those exerted on 2.5% DSPE-PEG-PDP/97.5% POPC vesicles initiating tLBM formation illustrates that the DSPE-PEG-PDP functional groups clearly play a role in anchoring vesicles to the surface. Furthermore, DSPE-PEG-PDP incorporation in vesicles may additionally (i) increase vesicle-substrate interactions leading to higher vesicle deformations[54] required for vesicle rupture, (ii) change vesicle–vesicle interactions due to the presence of PEG,[72,73] and/or (iii) change the bending rigidity of vesicles[74] leading to a lower tolerable vesicle deformation and a higher probability that tip penetration will lead to vesicle rupture and tLBM formation.

Minimum Forces Inducing tLBM Formation as a Function of DSPE-PEG-PDP Composition. From the above results, it is clear that external force in the absence of chemical functional groups on lipids in vesicles does not lead to tLBM formation on TS Au. While it is difficult to quantify forces exerted on the surface by the tip during AFM tapping-mode scanning, force spectroscopy precisely controls the force applied on a sample surface with an accuracy of a few piconewtons. The trigger for tip retraction can be set to a user-defined force, the trigger force, which the system measures between tip and sample surface. Since an AFM tip retracts at the user-defined trigger force, the trigger force is the maximum force exerted by an AFM tip on sample surfaces. In order to elucidate mechanisms, first we examine how DSPE-PEG-PDP functional lipid concentration affects vesicle rupture/tLBM formation on TS Au by performing AFM force spectroscopy with variable trigger forces, 0.5–2.5 nN, for three different DSPE-PEG-PDP compositions in vesicles incubated on TS Au. Force maps were acquired in 32 × 32 arrays on 1 μm × 1 μm regions on TS Au immediately after 30 min incubation. After acquiring force maps, AFM topography images were acquired in a 5 μm × 5 μm area with the 1 μm × 1 μm force mapped region in the center. This allows for examination of how the surface evolves as a result of the applied trigger force and compare with regions that did not interact with the AFM tip.

Figure 4a–c shows 5 μm × 5 μm AFM topography images after force spectroscopy with a trigger force of 1.2, 1.1, and 1.0 nN on TS Au after exposure to vesicles composed of 2.5% DSPE-PEG-PDP/97.5% POPC. Note: these were acquired on three different regions of the sample surface. Figure 4d–f shows 5 μm × 5 μm AFM topography images after force spectroscopy with a trigger force of 0.9, 0.8, and 0.7 nN on TS Au after

dx.doi.org/10.1021/la300127m | Langmuir 2012, 28, 7417–7427

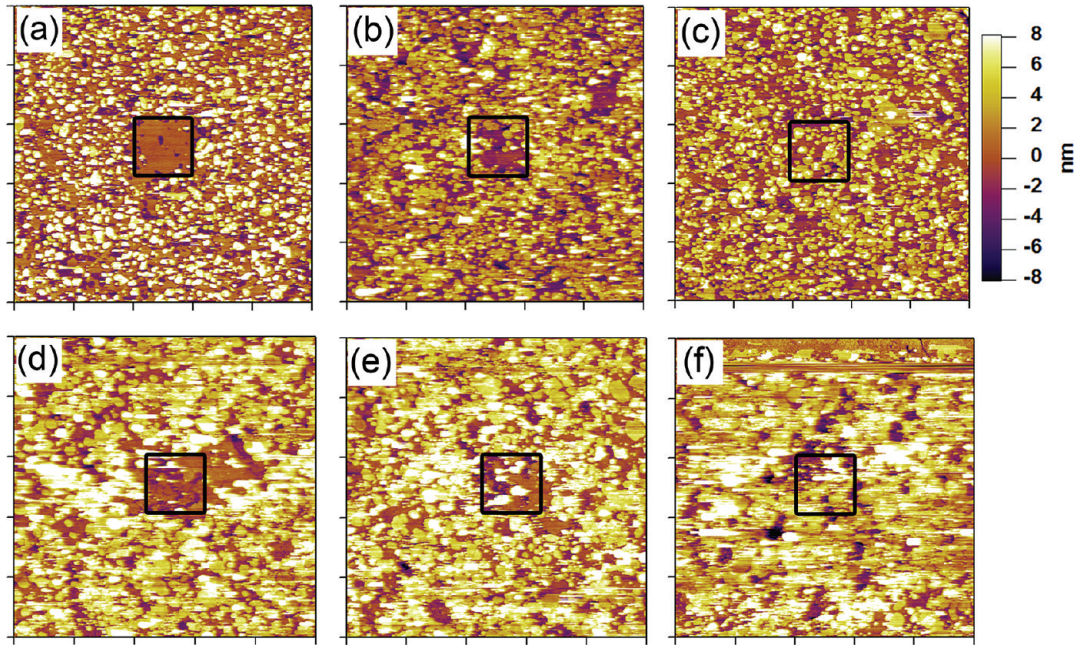

Figure 4. 5 μm × 5 μm AFM topography images of TS Au incubated with 2.5% DSPE-PEG-PDP/97.5% POPC vesicles acquired after 32 × 32 arrays force maps with a trigger force of (a) 1.2 nN, (b) 1.1 nN, and (c) 1.0 nN were obtained in the 1 μm × 1 μm region highlighted with a black square. 5 μm × 5 μm AFM topography images of TS Au incubated with 5% DSPE-PEG-PDP/95% POPC acquired after 32 × 32 arrays force maps with a trigger force of (d) 0.9 nN, (e) 0.8 nN, and (f) 0.7 nN were obtained in the 1 μm × 1 μm region highlighted with a black square.

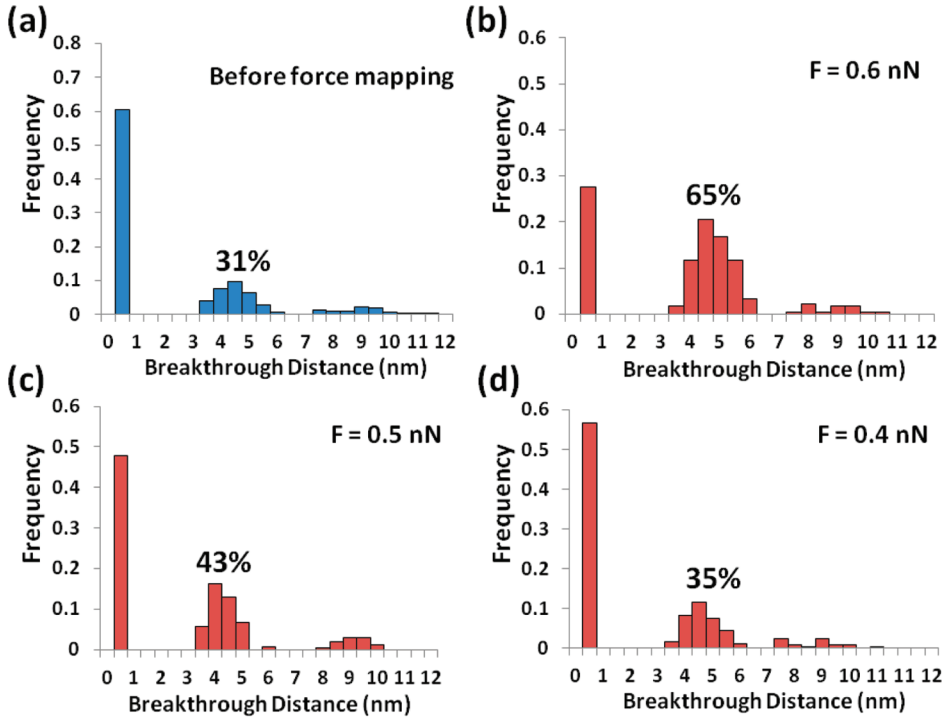

Figure 5. Histograms of measured breakthrough distances from force spectroscopy data that was acquired with a trigger force of 5 nN after 30 min incubation of vesicles composed of 10% DSPE-PEG-PDP/90% POPC on TS Au before (blue) (a) and after (red) a force map with a lower trigger force was acquired. The lower trigger force was (b) 0.6 nN, (c) 0.5 nN and (d) 0.4 nN.

exposure to vesicles composed of 5% DSPE-PEG-PDP/95% POPC. These were also acquired in three different regions of the sample surface. In the AFM images of Figure 4a,d, the regions in the black squares exhibit a surface predominantly covered with tLBM, while neighboring regions outside the force mapped area are mainly covered with adsorbed vesicles. When the trigger force was lowered by 0.1 nN, the force mapped region only shows partial tLBM formation coexisting with adsorbed vesicles, as observed in the AFM images of Figure 4b,e. When the trigger force is further lowered by 0.1 nN, there is no significant difference observed in AFM images between the force mapped region and the neighboring regions shown in Figure 4c,f, indicating that 1.1 nN and 0.8 nN are approximately the critical forces required for facilitating POPC

dx.doi.org/10.1021/la300127m | *Langmuir* 2012, 28, 7417−7427

vesicle rupture with 2.5% and 5% DSPE-PEG-PDP, respectively, on TS Au. Note that the critical force does not change when we decrease the array size to 16 × 16 (pixel area of 62.5 × 62.5 nm^2), and thus it only takes a few tip−surface interactions to lead to the rupture of vesicles. (See Supporting Information Figure S4.) Also it is important to note that the breakthrough force for tLBMs composed of POPC and DSPE-PEG-PDP is approximately 1.5 nN[42] and even higher for vesicles, as observed in Figure 2f, and thus vesicle rupture does not require complete penetration of vesicles by the AFM tip.

In the case of 10% DSPE-PEG-PDP/90% POPC vesicles, partial tLBM formation occurs over a considerable fraction of the surface during 30 min incubation at room temperature (for example, see Figure 1b). Thus we statistically monitored the evolution of surface features due to applied AFM tip forces by measuring breakthrough distances on 1 μm × 1 μm regions before and after a variable trigger force was applied to the surface by an AFM tip. These experiments were conducted by first acquiring a force map with a 5 nN trigger force, sufficient to measure breakthrough events and analyze surface coverage of tLBM and adsorbed vesicle before AFM tip−surface interactions. Then the AFM tip was translated to another representative region on the sample surface, and another 1 μm × 1 μm region was subjected to a smaller trigger force by the AFM tip. The smaller trigger force was varied from 1.0 nN to 0.35 nN. A force map was acquired on this same region with a trigger force of 5 nN, and breakthrough distances were measured to see how surface features evolved due to tip−surface interactions with the smaller trigger force.

Probabilities of observing breakthrough distances that correspond to bare Au, tLBMs, and vesicles were calculated from the force mapping data sets. For example, force−distance curves exhibiting a breakthrough distance of 4.4 ± 0.5 nm are classified as tLBM, and histograms provide information on the probability of observing these features. In order to examine sample uniformity before force mapping with the smaller trigger force, a few regions were measured on the sample surface with the 5 nN trigger force and were averaged from five different samples. Histograms showing the frequency of breakthrough events as a function of breakthrough distance that were determined from force−distance curves are shown for the initial 5 nN force map in Figure 5a. Features corresponding to tLBMs after incubating vesicles containing 10% DSPE-PEG-PDP on TS Au constituted 31% ± 6% (1 σ) of the observed features in measured force−distance curves. Thus, on average, the 30 min incubation period leads to approximately one-third of the sample surface covered with tLBMs. Histograms showing the frequency of breakthrough events as a function of breakthrough distance that were determined from force−distance curves are also shown for measurements acquired after the 0.6 nN force map (Figure 5b), after the 0.5 nN force map (Figure 5c), and after the 0.4 nN force map (Figure 5d). The trigger force of 0.6 nN led to an increase in the percentage of features corresponding to a tLBM from 31% to 65%. The trigger force of 0.5 nN, shown in Figure 5c, led to an increase in the percentage of features corresponding to a tLBM from 31% to 43%. However, when the trigger force was lowered to 0.4 nN, the percentage of force−distance curves corresponding to tLBMs had only a slight increase from 31% to 35% (Figure 5d), which does not constitute a significant increase when considering the standard deviation of the measurements. Thus, the trigger force corresponding to a measurable change in tLBM coverage due to force mapping was found to be approximately 0.5 nN for vesicles with 10% DSPE-PEG-PDP. This is approximately half the value of the trigger force required for 2.5% DSPE-PEG-PDP/97.5% POPC vesicles. A similar force mapping analysis was conducted for samples with vesicles composed of 2.5% DSPE-PEG-PDP/97.5% POPC on TS Au in order to see whether this process gives the same results as our analysis using AFM imaging to determine the critical force. The critical force quantified by the force mapping method for rupturing vesicles of 2.5% DSPE-PEG-PDP/97.5% POPC is 1.1 ± 0.1 nN, which is the same as the AFM imaging results shown in Figure 4a−c. (See Supporting Information Figure S5 for histogram plots before and after applying smaller trigger forces.)

Vesicles with 0% DSPE-PEG-PDP (pure POPC vesicles) do not remain on TS Au under applied force, and the critical trigger forces needed to rupture POPC vesicles containing 2.5%, 5% and 10% DSPE-PEG-PDP are 1.1, 0.8, and 0.5 nN, respectively; thus, vesicles with higher concentrations of functional lipids require a lower external force to facilitate tLBM formation on TS Au. Table 1 summarizes the critical trigger force for inducing vesicle rupture as a function of the DSPE-PEG-PDP concentration. Increases in vesicle-substrate interactions have previously been reported to lead to vesicle rupture at lower vesicle concentrations on surfaces, and it was hypothesized that the increased vesicle−substrate interactions lead to larger deformation of vesicles.[46,48,49] For vesicles of fixed size, theoretical models have varied the degree of interaction between vesicles and substrate and examined vesicle deformation as a function of this interaction.[55] Higher vesicle−substrate interactions lead to larger vesicle deformations that can be quantified with a bending angle. Vesicles having a large bending angle can minimize surface free energy via pore formation since, as the bending angle increases, the deformation energy becomes very high at the edges of vesicles.[49] This leads to an increase in the probability of vesicle rupture in Monte Carlo simulations.[54] Our results showing that the critical force needed to initiate vesicle rupture decreases as DSPE-PEG-PDP concentration increases are in agreement with this hypothesis. Au−thiolate bond formation between DSPE-PEG-PDP lipids and TS Au substrates increases the chemical affinity between vesicles and the TS Au substrate; thus as more functional groups are incorporated in vesicles, the vesicle−substrate contact area is expected to increase leading to higher deformation of vesicles. Specifically, when 10% DSPE-PEG-PDP is incorporated in vesicles, vesicles are expected to have larger deformation than when 2.5% DSPE-PEG-PDP is incorporated in POPC vesicles on TS Au, since there are more possible bonding sites between vesicles and TS Au. A schematic illustrating the proposed relationship between vesicle deformation and DSPE-PEG-PDP concentration is shown in Figure 6. Larger vesicle deformations destabilize vesicles, and

Table 1. List of Vesicle Rupture Critical Force as a Function of DSPE-PEG-PDP Concentration in POPC Vesicles

vesicle composition	vesicle rupture critical force
0% DSPE-PEG-PDP/100% POPC	no tLBM formation under external force
2.5% DSPE-PEG-PDP/97.5% POPC	1.1 ± 0.1 nN
5% DSPE-PEG-PDP/95% POPC	0.8 ± 0.1 nN
10% DSPE-PEG-PDP/90% POPC	0.5 ± 0.1 nN
2.5% DSPE-PEG-PDP/97.5% POPC (5 mM $CaCl_2$)	0.6 ± 0.1 nN

dx.doi.org/10.1021/la300127m | Langmuir 2012, 28, 7417−7427

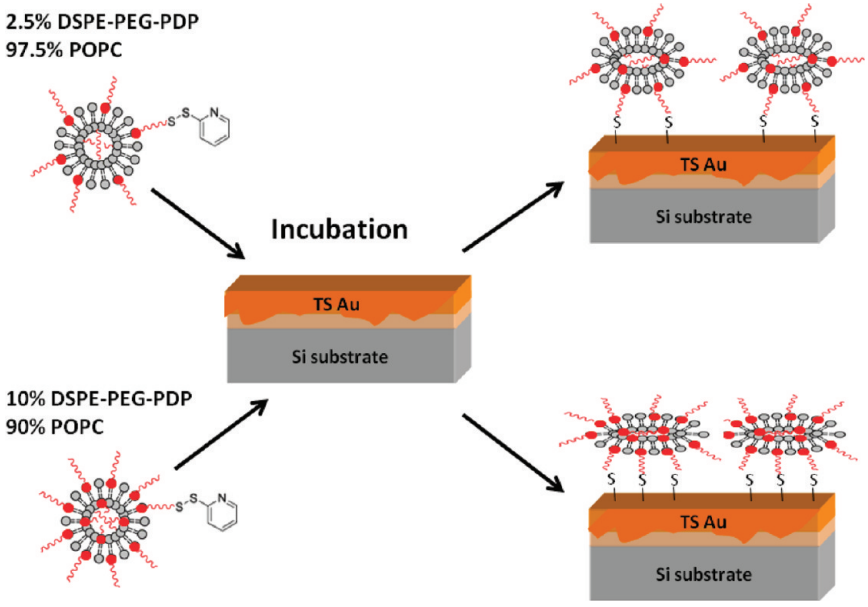

Figure 6. Scheme of TS Au after exposure to vesicles with lipid mixtures of POPC (gray) and DSPE-PEG-PDP (red).

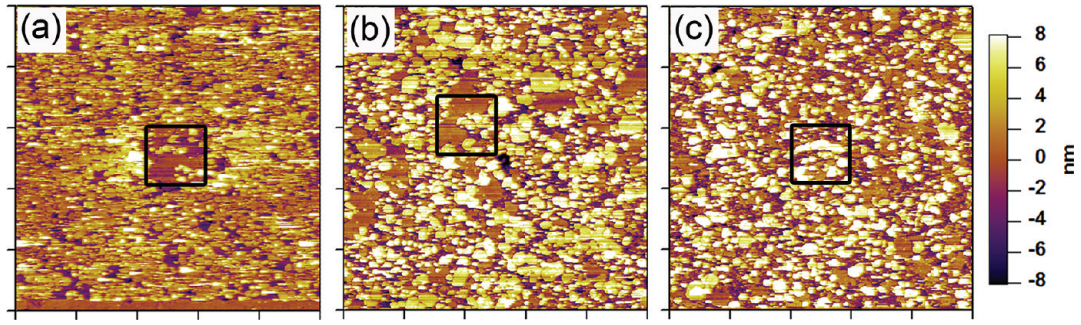

Figure 7. 5 μm × 5 μm AFM topography images of TS Au after incubation with 2.5% DSPE-PEG-PDP/97.5% POPC and imaged in the presence of 5 mM Ca^{2+} in HEPES buffer. Images were acquired after force spectroscopy was performed in 32 × 32 arrays in 1 μm × 1 μm regions (outlined with black squares). The trigger force was (a) 0.75 nN, (b) 0.6 nN, and (c) 0.5 nN.

thus lower external forces would be needed for vesicle rupture, as is observed in force spectroscopy measurements. However, as mentioned previously, it is also possible that the incorporation of PEG functionalized lipids may modify vesicle−vesicle interactions or change the bending rigidity of vesicles. Thus we analyzed whether POPC vesicles with 2.5% DSPE-PEG-PDP and 7.5% DSPE-PEG formed tLBMs at the same or different critical forces as POPC vesicles with 2.5% DSPE-PEG-PDP alone. We found that the additional unfunctionalized DSPE-PEG groups actually hindered tLBM formation (see Supporting Information Figure S6). Forces of 1.1 nN and 2.5 nN did not lead to significant tLBM formation when 2.5% DSPE-PEG-PDP and 7.5% DSPE-PEG were incorporated in vesicles. Therefore PEG did not appear to play a role in tLBM formation here.

Effect of Osmotic Pressure. We also examined critical forces needed to induce vesicle rupture under conditions of osmotic pressure. Divalent ions, particularly calcium ions (Ca^{2+}),[47] are known to facilitate vesicle fusion for zwitterionic vesicles such as POPC[48] and LBM formation by modifying vesicle−vesicle interactions and direct interaction with lipids and substrates.[29,75−77] However, previous studies show that osmotic pressure does not promote vesicle fusion on Au. For example, Reimhult et al., found that vesicles adsorbed on oxidized Au surfaces remained intact and did not form LBM[51] under osmotic pressure created by 300 mM NaCl. Yet osmotic pressure may affect vesicle rupture when functional lipids are incorporated in vesicles on TS Au.

After the standard incubation process of 2.5% DSPE-PEG-PDP/97.5% POPC vesicles on TS Au, the solution was exchanged with HEPES buffer with Ca^{2+} (5 mM HEPES, pH 7.4, containing 150 mM NaCl and 5 mM $CaCl_2$). Force spectroscopy was performed with trigger forces between 0.5 and 1.0 nN over a 1 μm × 1 μm region immediately after incubation. Again, 5 μm × 5 μm AFM topography images were acquired after force mapping, and the regions where the force maps were acquired were outlined with black squares. When the trigger force was 0.75 nN, as shown in Figure 7a, tLBM formation is observed. When reduced further to 0.6 nN, partial tLBM formation is observed in the force mapped region, and there is a slight difference from the neighboring region (Figure 7b). When the trigger force was further decreased to 0.5 nN, the force mapped region and neighboring region did not exhibit significant differences in morphology, as observed in the AFM topography image of Figure 7c. Thus the critical trigger force to promote vesicle fusion in the presence of osmotic pressure is approximately 0.6 nN. This is a reduction from 1.1 nN for 2.5% DSPE-PEG-PDP/97.5% POPC vesicles without osmotic

dx.doi.org/10.1021/la300127m | *Langmuir* 2012, 28, 7417−7427

pressure (see Table 1). Though osmotic pressure does not independently promote LBM on Au, as shown in previous studies, here we demonstrate that it does decrease the external force needed to promote vesicle rupture when functional lipids are present. It has previously been reported that external osmotic pressure leads to shrinkage and deformation of vesicles that facilitates rupture.[51] This is consistent with our hypothesis that higher vesicle deformations lead to rupture, and thus the force induced by the AFM tip leading to rupture is lower in the presence of osmotic pressure than that for vesicles without an osmotic gradient because vesicles are initially under a greater deformation.

CONCLUSION

Incorporation of functional lipids (DSPE-PEG-PDP) in POPC vesicles and resulting Au-thiolate bond formation is found to lead to tLBM on TS Au surfaces. The surface coverage of tLBM that spontaneously forms on Au after 30 min incubation is dependent on the concentration of functional lipids in vesicles. Critical forces initiating vesicle rupture as a function of the functional lipids composition in vesicles and with osmotic pressure were quantified using AFM force spectroscopy. We determined that the required forces initiating vesicle rupture monotonically decrease as functional lipid composition increases. The functional lipids appear to increase vesicle–substrate interactions, leading to a larger vesicle deformation with an increase in DSPE-PEG-PDP concentration in vesicles. Under osmotic pressure, the critical force for vesicle rupture also decreases, presumably also due to increased vesicle deformation. For applications where systems can withstand elevated temperature, incubation of vesicles on TS Au at 60 °C is a route to achieve large areas of uniform and continuous tLBMs on TS Au over 25 μm^2. In the case of room-temperature incubation, external force via an AFM tip effectively produces uniform tLBMs on TS Au. This strategy can be used to form membrane arrays on selective regions of a sample surface with varying lipid compositions and transmembrane proteins. Surface patterning of membrane arrays could be used for high-throughput analysis of membrane–protein interactions. In addition, tailoring surface chemistry on vesicle surfaces is a route for engineering specific vesicle–surface interactions that can lead to localized rupture in the presence of external perturbations. Combined with the method to quantify forces necessary for vesicle rupture introduced here, the results have potential for many applications such as designing and probing external triggers for effective release of drug in liposome carriers.

ASSOCIATED CONTENT

Supporting Information

S1: AFM image of bare TS Au; line profile corresponding to Figure 1a; representative force–distance curve obtained on tLBM region formed by incubation at 60 °C; and line profile across a region in Figure 1c. S2: AFM topography images of uniform tLBMs formed by continuous AFM scanning on TS Au surface after exposure to vesicles composed of 2.5% DSPE-PEG-PDP/97.5% POPC at three different positions and breakthrough distance histograms of 32 × 32 arrays, 16 × 16 arrays, and 8 × 8 arrays force mapping with the trigger force of 5 nN obtained corresponding to the three AFM imaging locations. S3: AFM topography images of POPC vesicles exposed to oxygen plasma cleaned TS Au acquired after the treatment of 32 × 32 arrays force mapping with the trigger force of 5.0 nN and 1.0 nN, and the corresponding force–distance curves obtained on the force mapped region. S4: Histograms of breakthrough distance on TS Au exposed to vesicles composed of 2.5% DSPE-PEG-PDP/97.5% POPC before and after the treatment of 16 × 16 arrays force mapping with the trigger force of 1.3 nN and 1.0 nN. S5: Breakthrough distance histograms of measured breakthrough distances from force spectroscopy data that was acquired with a trigger force of 5 nN from vesicles composed of 2.5% DSPE-PEG-PDP/97.5% POPC exposed to TS Au before and after the treatment of a force map with a lower trigger force of 1.2 nN and 1.0 nN. S6: AFM topography images of TS Au after exposure to vesicles composed of 2.5% DSPE-PEG-PDP/7.5% DSPE-PEG/90% POPC obtained after force mapping with a trigger force of 1.1 nN and 2.5 nN. This material is available free of charge via the Internet at http://pubs.acs.org.

AUTHOR INFORMATION

Corresponding Author

*Telephone: (949) 824-6830; fax: (949) 824-2541; e-mail: rragan@uci.edu.

Notes

The authors declare no competing financial interest.

ACKNOWLEDGMENTS

We thank Asylum Research Technical Support (Asylum Research, Santa Barbara, CA) for valuable discussions regarding AFM force mapping. We also thank Dr. Mo Kebaili and Dr. Vu Phan (Integrated Nanosystems Research Facility, UC Irvine) for electron beam deposition of Au film. We acknowledge Dr. Wytze van der Veer for support at the UC Irvine Laser Spectroscopy Facility where DLS measurements were performed. This work was supported by the National Science Foundation (CHE-0748912).

REFERENCES

(1) Tamm, L. K.; McConnell, H. M. Supported Phospholipid Bilayers. *Biophys. J.* **1985**, *47*, 105–113.
(2) Sackmann, E.; Tanaka, M. Supported Membranes on Soft Polymer Cushions: Fabrication, Characterization and Applications. *Trends Biotechnol.* **2000**, *18*, 58–64.
(3) Tanaka, M.; Sackmann, E. Polymer-Supported Membranes as Models of the Cell Surface. *Nature* **2005**, *437*, 656–663.
(4) Merz, C.; Knoll, W.; Textor, M.; Reimhult, E. Formation of Supported Bacterial Lipid Membrane Mimics. *Biointerphases* **2008**, *3*, FA41–FA50.
(5) McConnell, H. M.; Watts, T. H.; Weis, R. M.; Brian, A. A. Supported Planar Membranes in Studies of Cell–Cell Recognition in the Immune System. *Biochim. Biophys. Acta, Rev. Biomembr.* **1986**, *864*, 95–106.
(6) Kloboucek, A.; Behrisch, A.; Faix, J.; Sackmann, E. Adhesion-Induced Receptor Segregation and Adhesion Plaque Formation: A Model Membrane Study. *Biophys. J.* **1999**, *77*, 2311–2328.
(7) Qi, S. Y.; Groves, J. T.; Chakraborty, A. K. Synaptic Pattern Formation During Cellular Recognition. *Proc. Natl. Acad. Sci. U.S.A.* **2001**, *98*, 6548–6553.
(8) Bruinsma, R.; Behrisch, A.; Sackmann, E. Adhesive Switching of Membranes: Experiment and Theory. *Phys. Rev. E* **2000**, *61*, 4253.
(9) Grakoui, A.; Bromley, S. K.; Sumen, C.; Davis, M. M.; Shaw, A. S.; Allen, P. M.; Dustin, M. L. The Immunological Synapse: A Molecular Machine Controlling T Cell Activation. *Science* **1999**, *285*, 221–227.
(10) Watts, T. H.; Gaub, H. E.; McConnell, H. M. T-Cell-Mediated Association of Peptide Antigen and Major Histocompatibility

Complex Protein Detected by Energy Transfer in an Evanescent Wave-Field. *Nature* **1986**, *320*, 179−181.
(11) Feigenson, G. W. Phase Diagrams and Lipid Domains in Multicomponent Lipid Bilayer Mixtures. *Biochim. Biophys. Acta, Biomembr.* **2009**, *1788*, 47−52.
(12) Wong, J. Y.; Majewski, J.; Seitz, M.; Park, C. K.; Israelachvili, J. N.; Smith, G. S.; Polymer-Cushioned Bilayers., I. A Structural Study of Various Preparation Methods Using Neutron Reflectometry. *Biophys. J.* **1999**, *77*, 1445−1457.
(13) Merzlyakov, M.; Li, E.; Gitsov, I.; Hristova, K. Surface-Supported Bilayers with Transmembrane Proteins: Role of the Polymer Cushion Revisited. *Langmuir* **2006**, *22*, 10145−10151.
(14) Lang, H.; Duschl, C.; Gratzel, M.; Vogel, H. Self-Assembly of Thiolipid Molecular Layers on Gold Surfaces: Optical and Electrochemical Characterization. *Thin Solid Films* **1992**, *210*−*211*, 818−821.
(15) Naumann, C. A.; Prucker, O.; Lehmann, T.; Ruhe, J.; Knoll, W.; Frank, C. W. The Polymer-Supported Phospholipid Bilayer: Tethering as a New Approach to Substrate−Membrane Stabilization. *Biomacromolecules* **2001**, *3*, 27−35.
(16) Cornell, B. A.; Krishna, G.; Osman, P. D.; Pace, R. D.; Wieczorek, L. Tethered-Bilayer Lipid Membranes as a Support for Membrane-Active Peptides. *Biochem. Soc. Trans.* **2001**, *29*, 613−617.
(17) Knoll, W.; Köper, I.; Naumann, R.; Sinner, E.-K. Tethered Bimolecular Lipid Membranes—A Novel Model Membrane Platform. *Electrochim. Acta* **2008**, *53*, 6680−6689.
(18) Junghans, A.; Koper, I. Structural Analysis of Tethered Bilayer Lipid Membranes. *Langmuir* **2010**, *26*, 11035−11040.
(19) Raguse, B.; Braach-Maksvytis, V.; Cornell, B. A.; King, L. G.; Osman, P. D. J.; Pace, R. J.; Wieczorek, L. Tethered Lipid Bilayer Membranes: Formation and Ionic Reservoir Characterization. *Langmuir* **1998**, *14*, 648−659.
(20) Miller, C.; Cuendet, P.; Grätzel, M. K^+ Sensitive Bilayer Supporting Electrodes. *J. Electroanal. Chem. Interfac.* **1990**, *278*, 175−192.
(21) Stelzle, M.; Weissmueller, G.; Sackmann, E. On the Application of Supported Bilayers as Receptive Layers for Biosensors with Electrical Detection. *J. Phys. Chem.* **1993**, *97*, 2974−2981.
(22) Sackmann, E. Supported Membranes: Scientific and Practical Applications. *Science* **1996**, *271*, 43−48.
(23) Spinke, J.; Yang, J.; Wolf, H.; Liley, M.; Ringsdorf, H.; Knoll, W. Polymer-Supported Bilayer on a Solid Substrate. *Biophys. J.* **1992**, *63*, 1667−1671.
(24) Knoll, W.; Park, H.; Sinner, E.-K.; Yao, D.; Yu, F. Supramolecular Interfacial Architectures for Optical Biosensing with Surface Plasmons. *Surf. Sci.* **2004**, *570*, 30−42.
(25) Gritsch, S.; Nollert, P.; Jahnig, F.; Sackmann, E. Impedance Spectroscopy of Porin and Gramicidin Pores Reconstituted into Supported Lipid Bilayers on Indium−Tin-Oxide Electrodes. *Langmuir* **1998**, *14*, 3118−3125.
(26) McBee, T. W.; Wang, L.; Ge, C.; Beam, B. M.; Moore, A. L.; Gust, D.; Moore, T. A.; Armstrong, N. R.; Saavedra, S. S. Characterization of Proton Transport across a Waveguide-Supported Lipid Bilayer. *J. Am. Chem. Soc.* **2006**, *128*, 2184−2185.
(27) Steinberg-Yfrach, G.; Liddell, P. A.; Hung, S.-C.; Moore, A. L.; Gust, D.; Moore, T. A. Conversion of Light Energy to Proton Potential in Liposomes by Artificial Photosynthetic Reaction Centres. *Nature* **1997**, *385*, 239−241.
(28) Steinberg-Yfrach, G.; Rigaud, J.-L.; Durantini, E. N.; Moore, A. L.; Gust, D.; Moore, T. A. Light-Driven Production of ATP Catalysed by F_0F_1-ATP Synthase in an Artificial Photosynthetic Membrane. *Nature* **1998**, *392*, 479−482.
(29) Richter, R. P.; Berat, R.; Brisson, A. R. Formation of Solid-Supported Lipid Bilayers: An Integrated View. *Langmuir* **2006**, *22*, 3497−3505.
(30) Leonenko, Z. V.; Carnini, A.; Cramb, D. T. Supported Planar Bilayer Formation by Vesicle Fusion: The Interaction of Phospholipid Vesicles with Surfaces and the Effect of Gramicidin on Bilayer Properties Using Atomic Force Microscopy. *Biochim. Biophys. Acta, Biomembr.* **2000**, *1509*, 131−147.
(31) Garcia-Manyes, S.; Oncins, G.; Sanz, F. Effect of Ion-Binding and Chemical Phospholipid Structure on the Nanomechanics of Lipid Bilayers Studied by Force Spectroscopy. *Biophys. J.* **2005**, *89*, 1812−1826.
(32) Cremer, P. S.; Boxer, S. G. Formation and Spreading of Lipid Bilayers on Planar Glass Supports. *J. Phys. Chem. B* **1999**, *103*, 2554−2559.
(33) Schonherr, H.; Johnson, J. M.; Lenz, P.; Frank, C. W.; Boxer, S. G. Vesicle Adsorption and Lipid Bilayer Formation on Glass Studied by Atomic Force Microscopy. *Langmuir* **2004**, *20*, 11600−11606.
(34) Keller, C. A.; Kasemo, B. Surface Specific Kinetics of Lipid Vesicle Adsorption Measured with a Quartz Crystal Microbalance. *Biophys. J.* **1998**, *75*, 1397−1402.
(35) Steinem, C.; Janshoff, A.; Ulrich, W.-P.; Sieber, M.; Galla, H.-J. Impedance Analysis of Supported Lipid Bilayer Membranes: A Scrutiny of Different Preparation Techniques. *Biochim. Biophys. Acta, Biomembr.* **1996**, *1279*, 169−180.
(36) Munro, J. C.; Frank, C. W. Adsorption of Lipid-Functionalized Poly(ethylene glycol) to Gold Surfaces as a Cushion for Polymer-Supported Lipid Bilayers. *Langmuir* **2004**, *20*, 3339−3349.
(37) Lingler, S.; Rubinstein, I.; Knoll, W.; Offenhausser, A. Fusion of Small Unilamellar Lipid Vesicles to Alkanethiol and Thiolipid Self-Assembled Monolayers on Gold. *Langmuir* **1997**, *13*, 7085−7091.
(38) Naumann, R.; Schiller, S. M.; Giess, F.; Grohe, B.; Hartman, K. B.; Karcher, I.; Koper, I.; Lubben, J.; Vasilev, K.; Knoll, W. Tethered Lipid Bilayers on Ultraflat Gold Surfaces. *Langmuir* **2003**, *19*, 5435−5443.
(39) Wagner, M. L.; Tamm, L. K. Tethered Polymer-Supported Planar Lipid Bilayers for Reconstitution of Integral Membrane Proteins: Silane-Polyethyleneglycol-Lipid as a Cushion and Covalent Linker. *Biophys. J.* **2000**, *79*, 1400−1414.
(40) Shen, W. W.; Boxer, S. G.; Knoll, W.; Frank, C. W. Polymer-Supported Lipid Bilayers on Benzophenone-Modified Substrates. *Biomacromolecules* **2000**, *2*, 70−79.
(41) Chen, M.; Li, M.; Brosseau, C. L.; Lipkowski, J. AFM Studies of the Effect of Temperature and Electric Field on the Structure of a DMPC-Cholesterol Bilayer Supported on a Au(111) Electrode Surface. *Langmuir* **2009**, *25*, 1028−1037.
(42) Wang, X.; Shindel, M. M.; Wang, S.-W.; Ragan, R. A Facile Approach for Assembling Lipid Bilayer Membranes on Template-Stripped Gold. *Langmuir* **2010**, *26*, 18239−18245.
(43) Florin, E.-L.; Moy, V. T.; Gaub, H. E. Adhesion Forces between Individual Ligand−Receptor Pairs. *Science* **1994**, *264*, 415−417.
(44) Kada, G.; Kienberger, F.; Hinterdorfer, P. Atomic Force Microscopy in Bionanotechnology. *Nano Today* **2008**, *3*, 12−19.
(45) Hinterdorfer, P.; Dufrene, Y. F. Detection and Localization of Single Molecular Recognition Events Using Atomic Force Microscopy. *Nat. Methods* **2006**, *3*, 347−355.
(46) Lipowsky, R.; Seifert, U. Adhesion of Vesicles and Membranes. *Mol. Cryst. Liq. Cryst.* **1991**, *202*, 17−25.
(47) Reviakine, I.; Brisson, A. Formation of Supported Phospholipid Bilayers from Unilamellar Vesicles Investigated by Atomic Force Microscopy. *Langmuir* **2000**, *16*, 1806−1815.
(48) Richter, R.; Mukhopadhyay, A.; Brisson, A. Pathways of Lipid Vesicle Deposition on Solid Surfaces: A Combined QCM-D and AFM Study. *Biophys. J.* **2003**, *85*, 3035−3047.
(49) Zhdanov, V. P.; Kasemo, B. Comments on Rupture of Adsorbed Vesicles. *Langmuir* **2001**, *17*, 3518−3521.
(50) Dimitrievski, K. Deformation of Adsorbed Lipid Vesicles as a Function of Vesicle Size. *Langmuir* **2010**, *26*, 3008−3011.
(51) Reimhult, E.; Hook, F.; Kasemo, B. Intact Vesicle Adsorption and Supported Biomembrane Formation from Vesicles in Solution: Influence of Surface Chemistry, Vesicle Size, Temperature, and Osmotic Pressure. *Langmuir* **2003**, *19*, 1681−1691.
(52) Johnson, J. M.; Ha, T.; Chu, S.; Boxer, S. G. Early Steps of Supported Bilayer Formation Probed by Single Vesicle Fluorescence Assays. *Biophys. J.* **2002**, *83*, 3371−3379.

(53) Reimhult, E.; Hook, F.; Kasemo, B. Vesicle Adsorption on SiO_2 and TiO_2: Dependence on Vesicle Size. *J. Chem. Phys.* **2002**, *117*, 7401−7404.
(54) Dimitrievski, K.; Zach, M.; Zhdanov, V. P.; Kasemo, B. Imaging and Manipulation of Adsorbed Lipid Vesicles by an AFM Tip: Experiment and Monte Carlo Simulations. *Colloids Surf., B* **2006**, *47*, 115−125.
(55) Zhdanov, V. P.; Dimitrievski, K.; Kasemo, B. Adsorption and Spontaneous Rupture of Vesicles Composed of Two Types of Lipids. *Langmuir* **2006**, *22*, 3477−3480.
(56) Sharma, S.; Palanisamy, V.; Mathisen, C.; Schmidt, M.; Gimzewski, J. K. Exosomes—Biological Liposomes as Potential Drug Delivery Agents. *Global J. Phys. Chem.* **2011**, *2*, 125−128.
(57) van den Boorn, J. G.; Schlee, M.; Coch, C.; Hartmann, G. siRNA Delivery with Exosome Nanoparticles. *Nat. Biotechnol.* **2011**, *29*, 325−326.
(58) Balazs, D. A.; Godbey, W. Liposomes for Use in Gene Delivery. *J. Drug Delivery* **2011**, *2011*, 1−12.
(59) Ibsen, S.; Benchimol, M.; Simberg, D.; Schutt, C.; Steiner, J.; Esener, S. A Novel Nested Liposome Drug Delivery Vehicle Capable of Ultrasound Triggered Release of Its Payload. *J. Controlled Release* **2011**, *155*, 358−366.
(60) Evjen, T. J.; Nilssen, E. A.; Barnert, S.; Schubert, R.; Brandl, M.; Fossheim, S. L. Ultrasound-Mediated Destabilization and Drug Release from Liposomes Comprising Dioleoylphosphatidylethanolamine. *Eur. J. Pharm. Sci.* **2011**, *42*, 380−386.
(61) Yudina, A.; de Smet, M.; Lepetit-Coiffé, M.; Langereis, S.; Van Ruijssevelt, L.; Smirnov, P.; Bouchaud, V.; Voisin, P.; Grüll, H.; Moonen, C. T. W. Ultrasound-Mediated Intracellular Drug Delivery Using Microbubbles and Temperature-Sensitive Liposomes. *J. Controlled Release* **2011**, *155*, 442−448.
(62) McMahon, H. T.; Gallop, J. L. Membrane Curvature and Mechanisms of Dynamic Cell Membrane Remodelling. *Nature* **2005**, *438*, 590−596.
(63) Lee, H. J.; Peterson, E. L.; Phillips, R.; Klug, W. S.; Wiggins, P. A. Membrane Shape as a Reporter for Applied Forces. *Proc. Natl. Acad. Sci.U.S.A.* **2008**, *105*, 19253−19257.
(64) Hope, M. J.; Bally, M. B.; Webb, G.; Cullis, P. R. Production of Large Unilamellar Vesicles by a Rapid Extrusion Procedure. Characterization of Size Distribution, Trapped Volume and Ability to Maintain a Membrane Potential. *Biochim. Biophys. Acta, Biomembr.* **1985**, *812*, 55−65.
(65) Lee, S.; Bae, S.-S.; Medeiros-Ribeiro, G.; Blackstock, J. J.; Kim, S.; Stewart, D. R.; Ragan, R. Scanning Tunneling Microscopy of Template-Stripped Au Surfaces and Highly Ordered Self-Assembled Monolayers. *Langmuir* **2008**, *24*, 5984−5987.
(66) Ragan, R.; Ohlberg, D.; Blackstock, J. J.; Kim, S.; Williams, R. S. Atomic Surface Structure of UHV-Prepared Template-Stripped Platinum and Single-Crystal Platinum(111). *J. Phys. Chem. B* **2004**, *108*, 20187−20192.
(67) Hutter, J. L.; Bechhoefer, J. Calibration of Atomic-Force Microscope Tips. *Reviews Sci. Instrum.* **1993**, *64*, 1868.
(68) Lewis, B. A.; Engelman, D. M. Lipid Bilayer Thickness Varies Linearly with Acyl Chain Length in Fluid Phosphatidylcholine Vesicles. *J. Mol. Biol.* **1983**, *166*, 211−217.
(69) Goksu, E. I.; Longo, M. L. Ternary Lipid Bilayers Containing Cholesterol in a High Curvature Silica Xerogel Environment. *Langmuir* **2010**, *26*, 8614−8624.
(70) Ohki, S.; Arnold, K. A Mechanism for Ion-Induced Lipid Vesicle Fusion. *Colloids Surf., B* **2000**, *18*, 83−97.
(71) Ngwa, W.; Chen, K.; Sahgal, A.; Stepanov, E. V.; Luo, W. Nanoscale Mechanics of Solid-Supported Multilayered Lipid Films by Force Measurement. *Thin Solid Films* **2008**, *516*, 5039−5045.
(72) Barry, R, L. Polymer-Induced Membrane Fusion: Potential Mechanism and Relation to Cell Fusion Events. *Chem. Phys. Lipids* **1994**, *73*, 91−106.
(73) Hui, S. W.; Kuhl, T. L.; Guo, Y. Q.; Israelachvili, J. Use of Poly(ethylene glycol) to Control Cell Aggregation and Fusion. *Colloids Surf., B* **1999**, *14*, 213−222.
(74) Evans, E.; Rawicz, W. Elasticity of "Fuzzy" Biomembranes. *Phys. Rev. Lett.* **1997**, *79*, 2379−2382.
(75) Ekeroth, J.; Konradsson, P.; Hook, F. Bivalent-Ion-Mediated Vesicle Adsorption and Controlled Supported Phospholipid Bilayer Formation on Molecular Phosphate and Sulfate Layers on Gold. *Langmuir* **2002**, *18*, 7923−7929.
(76) Nollert, P.; Kiefer, H.; Jähnig, F. Lipid Vesicle Adsorption Versus Formation of Planar Bilayers on Solid Surfaces. *Biophys. J.* **1995**, *69*, 1447−1455.
(77) Jass, J.; Tjarnhage, T.; Puu, G. From Liposomes to Supported, Planar Bilayer Structures on Hydrophilic and Hydrophobic Surfaces: An Atomic Force Microscopy Study. *Biophys. J.* **2000**, *79*, 3153−3163.